Neutron-scattering study of antiferromagnetism in $YBa_2Cu_3O_{6.15}$

S. Shamoto and M. Sato
Department of Physics, Nagoya University, Nagoya 464-01, Japan

J. M. Tranquada, B. J. Sternlieb, and G. Shirane
Physics Department, Brookhaven National Laboratory, Upton, New York 11973
(Received 15 July 1993)

Both the static and dynamic properties of the antiferromagnetic state in $YBa_2Cu_3O_{6.15}$ have been reinvestigated by neutron scattering. The crystal studied exhibited a Néel temperature of 410 ± 3 K, with a continuous transition below 15 K to a magnetic structure with a doubled unit cell along the c axis. The Cu magnetic form factor has been extracted from magnetic Bragg peak intensities measured at 15 K, and it is shown to have the large anisotropy expected for a Cu $3d_{x^2-y^2}$ state. The form-factor anisotropy can explain much of the **Q** dependence of the inelastic magnetic cross section that has been observed in superconducting $YBa_2Cu_3O_{6+x}$. A search for the optical spin-wave modes at excitation energies up to 60 meV was unsuccessful. Analysis of acoustic spin-wave measurements yields an intralayer superexchange energy $J_\parallel$ of 120 ± 20 meV (without correction for quantum renormalization) with an anisotropy $\alpha_{xy} = (7 \pm 1) \times 10^{-4}$, and an effective next-nearest-layer exchange $J_{\perp 2}$ of 0.04 ± 0.01 meV. A lower limit for the intra-bilayer exchange, $J_{\perp 1}$, of 8 meV is established. Use of theoretical and experimental results for **Q**-integrated spin-wave intensities in the antiferromagnet, together with a crystal volume normalization based on phonon measurements, allows us to put previous measurements of spin fluctuations in superconducting $YBa_2Cu_3O_{6.6}$ on an absolute scale. The results for the superconductor are shown to be consistent with the relaxation rates determined by nuclear magnetic resonance.

I. INTRODUCTION

The properties of the antiferromagnetic state in insulating $YBa_2Cu_3O_{6+x}$ with $x \lesssim 0.4$ are of considerable interest both because this material is a nearly two-dimensional (2D) quantum antiferromagnet,[1,2] and because it is an important reference system for comparison with the superconducting phase that occurs for $x \gtrsim 0.4$.[3,4] Previous neutron-scattering studies have established the general nature of the magnetic ordering[5–9] and the spin-wave spectrum;[10–13] nevertheless, several important features require further characterization. In this paper we report a new set of measurements involving a single crystal with $x \approx 0.15$.

One of the surprising features of $YBa_2Cu_3O_{6+x}$ is the strong antiferromagnetic coupling between nearest-neighbor CuO_2 planes. This coupling, which splits the single-layer spin-wave excitations into acoustic and optical branches, survives even in the metallic phase.[14–18] To determine the strength of the coupling, one must first observe the optical modes, which have so far escaped detection. This objective was a major motivation for the present study. Unfortunately, despite a search covering excitation energies up to 60 meV, we have failed to detect the optical modes. This negative result, combined with measurements of the acoustic spin-wave modes, yields a lower limit for the effective nearest-layer exchange $J_{\perp 1}$ of 8 meV.

Our previous investigation of the acoustic spin waves involved a crystal with $x \approx 0.3$ and $T_N = 260$ K.[11] The present crystal, with $x \approx 0.15$, has a similar oxygen content to the one characterized by Rossat-Mignod and coworkers,[12,13] and its Néel temperature of 410 ± 3 K indicates a negligible degree of hole doping in the CuO_2 planes.[6] We have measured the acoustic spin waves at low temperature, and analyzed them in terms of a spin-wave model based on a simple three-dimensional spin Hamiltonian. By taking advantage of the focusing properties of the neutron spectrometer's resolution function, it has been possible to nearly resolve the steeply dispersing in-plane modes at an excitation energy of 42 meV. Resolution-corrected fits to the data yield an intralayer nearest-neighbor superexchange energy $J_\parallel$ of 120 ± 20 meV, without correction for quantum renormalization. At lower energies, the observed anisotropy gap of ~ 9 meV indicates an in-plane superexchange anisotropy α_{xy} of $(7 \pm 1) \times 10^{-4}$, while dispersion along Q_z is modeled by an effective next-nearest-layer exchange $J_{\perp 2}$ of 0.04 ± 0.01 meV.

New results concerning the static properties of the magnetic ordering have also been obtained. Of particular interest is our measurement and analysis of the Cu magnetic form factor. Previous measurements of the Cu form factor in La_2CuO_4 (Ref. 19) and $Sr_2CuO_2Cl_2$ (Ref. 20) have indicated some discrepancies with the theoretical result for a spherical spin density; however, they have not demonstrated the strong anisotropy that should be expected for a Cu $3d_{x^2-y^2}$ orbital. Our results clearly reveal this anisotopy, and are in reasonable agreement with the properly calculated form factor. A surprising result concerning the magnetic ordering is the finding that below 15 K our crystal exhibits a continuous tran-

sition to a magnetic structure with a doubled unit cell along the c axis. Such a transition was first observed in a crystal with nonuniform oxygen content by Kadowaki *et al.*,[21] and is commonly observed in $Nd_{1+y}Ba_{2-y}Cu_3O_{6+x}$ crystals,[22–25] but otherwise has not been observed in either crystals or powders of the Y compound.

Finally, as mentioned above, the antiferromagnetic state is a useful reference for the metallic phase of $YBa_2Cu_3O_{6+x}$. We compare the **Q**-integrated spin-wave intensities for the antiferromagnet with analogous measurements obtained previously for an $x = 0.6$ crystal with a superconducting transition temperature T_c of 53 K.[16] The difference in crystal volumes is accounted for by normalization to phonon intensities. The comparison allows an estimate of the absolute magnitude of the dynamical spin susceptibility in the superconducting material.

The rest of this paper is organized as follows. In the next section we discuss the experimental details, including sample preparation and characterization. Our results and analysis of the magnetic form factor follow in Sec. III. The spin-wave measurements and analysis are presented in Sec. IV, and Sec. V contains the comparison of integrated intensities. The relevant discussion is contained within each section.

II. EXPERIMENTAL PROCEDURE

A. Sample preparation

$YBa_2Cu_3O_{6+x}$ (1:2:3 phase) decomposes at about 1040 °C to Y_2BaCuO_5 (2:1:1 phase) and a liquid phase. Crystals of $YBa_2Cu_3O_{6+x}$ can be obtained by peritectic reaction when the mixture of 2:1:1 and the liquid phase is cooled through the decomposition temperature of 1:2:3. The morphology of the crystals depends on the diffusion rate of the 1:2:3 constituent in the liquid phase and the dissolution rate of the 2:1:1 phase relative to the rate of crystal growth, which is controlled by the cooling rate. When the cooling rate is too great relative to the diffusion rate, one obtains a crystal with many dislocations and a wide mosaic spread. A rapid cooling rate also makes it difficult to minimize inclusions of the 2:1:1 phase. Although gravity tends to separate the denser 2:1:1 particles from the liquid, the viscosity of the liquid is sufficient to retain a suspension of particles. Therefore, a very slow cooling rate was adopted for the crystal growth. Further details are reported in Ref. 26.

The inevitable small inclusions of the 2:1:1 phase are not all bad. Ideally, one would like to obtain a large, perfect crystal with no inclusions of the 2:1:1 phase. However, the oxygen content of a crystal must be adjusted by post-annealing, and experience has shown that it is increasingly difficult to control the oxygen content as flux inclusions are eliminated and the crystal perfection is increased. The present crystal, which was approximately $15 \times 10 \times 4$ mm^3 in size, was annealed under a vacuum of 2×10^{-2} Torr at 650 °C for 3 days. Although a deliberate search was not performed, no evidence of diffraction from the impurity phase was observed in any of our measurements (cf. Fig. 4).

B. Neutron-scattering measurements

The neutron-scattering measurements were carried out on the triple-axis spectrometers H4M and H8 at the High Flux Beam Reactor located at Brookhaven National Laboratory. The (002) reflection of pyrolytic graphite (PG) was used for both monochromator and analyzer, and PG filters were employed to suppress higher-order contamination in the diffracted beam. The elastic and inelastic measurements were generally taken with a fixed final neutron energy E_f of 14.7 or 30.5 meV. In measuring the magnetic Bragg peaks for the form-factor determination, two PG filters were used and the neutron energy was scanned while sitting on each reflection to test for multiple scattering effects. For the spin-wave measurements, the horizontal collimations were 40′-40′-80′-80′.

The 1:2:3 crystal was wrapped in Al foil, clamped to an Al plate, and sealed in a cylindrical Al sample can with He exchange gas. The crystal was oriented with a $[1\bar{1}0]$ axis vertical, so that (hhl) reflections lie in the horizontal scattering plane. The sample can was generally mounted in a Displex closed-cycle refrigerator, except for the study of the low-temperature magnetic transition, where a pumped-He cryostat was used.

C. Sample characterization

The room-temperature lattice parameters of the tetragonal unit cell were determined to be $a = 3.86$ Å and $c = 11.82$ Å by both x-ray and neutron diffraction measurements. To check the oxygen content x, integrated intensities for 21 independent Bragg reflections of the type (hhl) were collected in θ-2θ mode at a temperature of 15 K. (Several of the strongest reflections, which would be subject to the largest extinction correction, were not included in this set.) The structural parameters[3] z_{Cu2}, z_{O2}, z_{O4}, and z_{Ba}, along with the oxygen content x, were determined by performing a least-squares fit to the intensities, corrected for the Lorentz factor. Two other parameters, a scale factor and an extinction parameter, were also determined in the fitting procedure; Debye-Waller factors were neglected. A comparison of the observed and calculated structure factors is shown in Fig. 1. The fit yielded values of $x = 0.15$ and $z_{Cu2} = 0.3625$, with an R factor of 0.052. Employing the structural parameters determined by neutron powder diffraction studies[3,4] gave only a slight increase in the R factor, and indicated an uncertainty in x of ± 0.05.

The magnetic ordering behavior was determined by monitoring the temperature dependence of various magnetic Bragg peaks, as illustrated in Fig. 2. The power-law fit shown in the figure yields a Néel temperature of 407 K, whereas the intensities close to the transition indicate 410 ± 3 K. The spin structure corresponds to that shown in Fig. 3(a): a simple Néel structure with spins lying in the CuO_2 planes.[5] A second magnetic transition is observed below 15 K, in which the intensities of magnetic peaks of type $(\frac{1}{2}\,\frac{1}{2}\,l)$ decrease continuously, while new peaks of type $(\frac{1}{2}\,\frac{1}{2}\,l + \frac{1}{2})$ appear. The change in the pattern of magnetic peaks is illustrated in Fig. 4. Such a transition was first observed by Kadowaki *et al.*[21] in

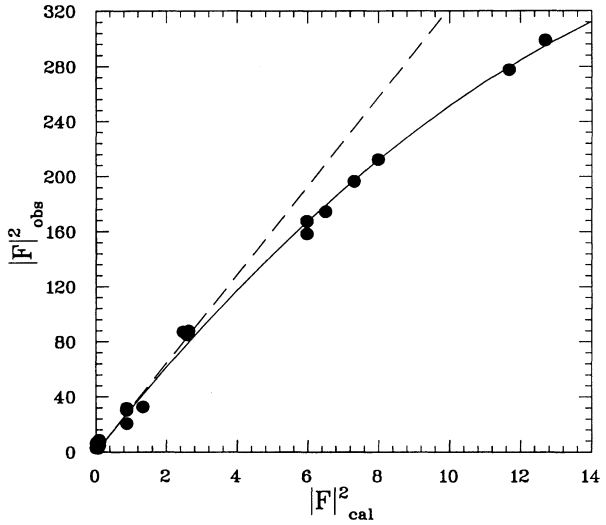

FIG. 1. Plot of the observed nuclear structure factor squared $|F|^2_{obs}$ versus the calculated squared structure factor $|F|^2_{cal}$. The solid line is of the form $y = Ax(1 - Bx)$, where A is a scale factor and B accounts for extinction.

a mixed-phase 1:2:3 crystal. The $l + \frac{1}{2}$ peaks can be accounted for by a magnetic domain with the spin structure indicated in Fig. 3(b): The magnetic unit cell is doubled along the c axis due to ferromagnetic coupling between bilayers through the "chain" layers. Kadowaki *et al.*[21] pointed out that besides a two domain model, one can account for the observed intensities equally well with a single homogeneous magnetic structure involving a linear combination of the two spin structures shown in Fig. 3, with an angle of 90° between the spin axes of the two component structures. In the resultant structure there is a rotation of the spin axis of one bilayer by an angle $+\alpha$, and an opposite rotation of $-\alpha$ in the neighboring

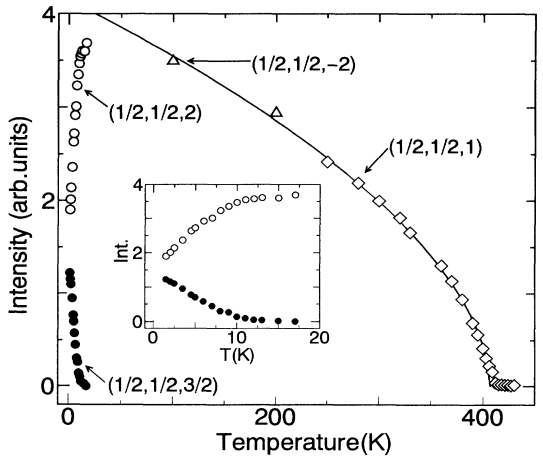

FIG. 2. Temperature dependence of magnetic Bragg peak intensities. The solid line is the result of a least-squares fit to a simple power law, $I \sim (T_N - T)^{2\beta}$ ($T_N = 407$ K, $\beta = 0.27$). The inset shows the temperature dependence of the $(\frac{1}{2}, \frac{1}{2}, 2)$ (open circles) and $(\frac{1}{2}, \frac{1}{2}, \frac{3}{2})$ (solid circles) peak intensities.

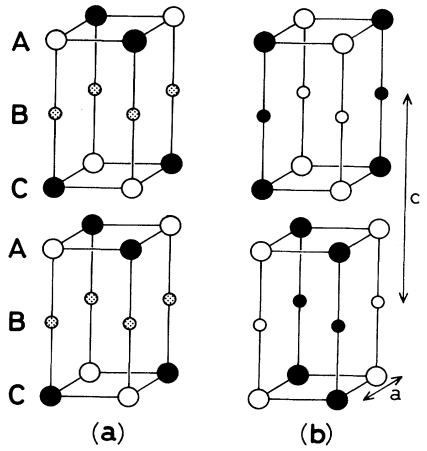

FIG. 3. (a) High-temperature magnetic structure corresponding to the $(\frac{1}{2}\ \frac{1}{2}\ l)$ (l = integer) reflections. Open and solid circles at Cu(2) sites in the CuO_2 planes represent mutually antiparallel spins oriented perpendicular to the c axis. Small shaded circles represent Cu(1) sites with no magnetic order. (b) Magnetic structure consistent with the low-temperature magnetic reflections at $(\frac{1}{2}\ \frac{1}{2}\ l + \frac{1}{2})$. Small circles represent the average moment and spin orientation on Cu(1) sites.

bilayers. The direction of spins on Cu(1) sites is rotated by $90° - \alpha$ relative to the directions in the neighboring planes. Applying the single-phase model to our measurements at 1.5 K, we obtain a moment of $(0.47 \pm 0.03)\mu_B$ on Cu(2) and $(0.005 \pm 0.002)\mu_B$ on Cu(1), with a turn angle $\alpha = 41.5° \pm 0.9°$.

The observation of the low-temperature transition came as something of a surprise. Except for the report by Kadowaki *et al.*,[21] the phase has not been detected in any other studies of $YBa_2Cu_3O_{6+x}$ by neutron diffraction or nuclear magnetic resonance (NMR). A slightly different low-temperature transition, in which the $(\frac{1}{2}\ \frac{1}{2}\ l)$ peaks decrease in intensity and diffuse scattering appears along the $(\frac{1}{2}\ \frac{1}{2}\ l)$ magnetic rod, has been observed in single-crystal neutron studies for $0.2 \lesssim x \lesssim 0.4$.[6,11] The doubled-unit-cell phase has been observed

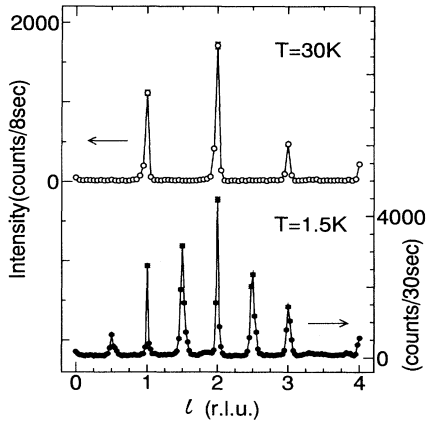

FIG. 4. Elastic scans along $\mathbf{Q} = (\frac{1}{2}, \frac{1}{2}, l)$ at 30 K ($> T_{N2}$) and 1.5 K ($< T_{N2}$). The solid lines are guides to the eye.

in $Nd_{1+y}Ba_{2-y}Cu_3O_{6+x}$,[22–25] but that system differs in containing a magnetic rare-earth element that can sit on both the Y and Ba sites.[27–29] The low-temperature phase has also been detected in Fe-doped $YBa_2Cu_3O_{6+x}$.[30] In the present case, the low-temperature transition may be related to the presence of a small fraction of magnetic Cu^{2+} ions on Cu(1) sites together with an absence of doped holes.[31,32] Such a configuration can occur if the occupied O(1) sites, between Cu(1) atoms, are isolated from one another. This condition appears to be destroyed for $x \approx 0$ [no occupied O(1) sites] or $x \gtrsim 0.2$ (added oxygens tend to cluster into chain fragments).

To avoid the influence of the low-temperature phase, the measurements discussed below were generally performed at temperatures of 15 K or greater.

III. MAGNETIC FORM FACTOR

The integrated intensities of the magnetic Bragg peaks are proportional to the square of the magnetic structure factor F_M, which in the present case can be written as

$$|F_M|^2 = \gamma_0^2 \langle \sin^2 \eta \rangle \mu^2 f^2(\mathbf{Q}) g^2(\mathbf{Q}), \tag{1}$$

where $\gamma_0 = 0.269 \times 10^{-12}$ cm, η is the angle between the spin direction and $\mathbf{Q}$, μ is the magnetic moment, $f(\mathbf{Q})$ is the magnetic form factor, and $g(\mathbf{Q})$ is a structure factor associated with the bilayer spin structure. The brackets around $\sin^2 \eta$ indicate an average over magnetic domains; with the spin direction perpendicular to the c axis, together with the tetragonal symmetry, we have

$$\langle \sin^2 \eta \rangle = \frac{1}{2}(1 + \cos^2 \beta), \tag{2}$$

where

$$\cos \beta = Q_z/Q. \tag{3}$$

The bilayer structure factor is given by

$$g(\mathbf{Q}) = 2 \sin(\pi z'_{Cu2} l), \tag{4}$$

where $z'_{Cu2} = 1 - 2z_{Cu2}$. Integrated intensities were measured for a series of magnetic Bragg peaks of the types $(\frac{1}{2}\frac{1}{2}l)$ and $(\frac{3}{2}\frac{3}{2}l)$ at a temperature of 15 K. The quantity $\mu f(\mathbf{Q})$ extracted from these measurements is plotted in Fig. 5. The points that deviate significantly from the general trend correspond to l values where the bilayer structure factor becomes quite small. At these positions the extracted values of $\mu f(\mathbf{Q})$ are quite sensitive to multiple scattering, measurement errors, and possible contributions to the spin density not centered on the Cu(2) sites.

The anisotropy of the form factor is quite striking. It is clear that the form factor depends strongly on the direction of $\mathbf{Q}$ as well as its magnitude. The main difference between the present results and earlier studies of La_2CuO_4 (Ref. 19) and $Sr_2CuO_2Cl_2$ (Ref. 20) is that we have extended the measurements to larger values of l. The theoretical form factor for a spherically averaged Cu $3d$ electronic spin density, indicated by the dashed line in the figure, is clearly inadequate. This discrepancy should have been anticipated,[33] since it has long been accepted

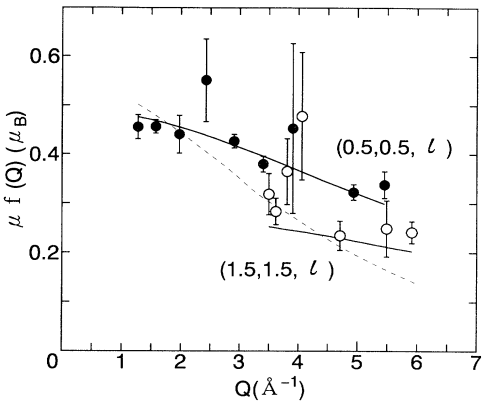

FIG. 5. The $\mathbf{Q}$ dependence of $\mu f(\mathbf{Q})$. The solid circles correspond to $(\frac{1}{2}\frac{1}{2}l)$ reflections, while open circles represent $(\frac{3}{2}\frac{3}{2}l)$ peaks. The solid line is the form factor for Cu $3d_{x^2-y^2}$, calculated as discussed in the text, while the dashed line is the form factor for a spherically averaged Cu $3d$ hole.

that the hole in the Cu $3d$ shell has $x^2 - y^2$ symmetry, which is quite far from being spherical.

We have calculated the $3d_{x^2-y^2}$ form factor using formulas given by Freeman.[34,35] Let $R_{3d}(r)$ be the radial component of the wave function of an atomic Cu $3d$ orbital. Defining the quantity $\langle j_n \rangle$ by

$$\langle j_n \rangle = \int_0^\infty R_{3d}^2(r) j_n(Qr) r^2 dr, \tag{5}$$

where j_n is a spherical Bessel function, the form factor can be written as

$$f(\mathbf{Q}) = \langle j_0 \rangle - \frac{5}{7}\left(1 - 3\cos^2\beta\right)\langle j_2 \rangle + \frac{9}{56}\left(1 - 10\cos^2\beta + \frac{35}{3}\cos^4\beta\right)\langle j_4 \rangle, \tag{6}$$

where $\cos\beta$ is given by Eq. (3). The radial wave function was computed using a program for atomic calculations based on the local-density approximation.[36] The calculated form factor is represented by the solid line in Fig. 5. The form factor has been scaled by the moment μ, whose value of $0.52\mu_B$ was determined by a least-squares fit to the data.

Past studies[7,8] have found that the low-temperature ordered moment scales with the Néel temperature. Because of the large value of T_N for the present crystal, we expect the moment to correspond to the maximum observable value; however, it is substantially lower than the maximum value of approximately $0.64\mu_B$ reported previously.[7,8] A major reason for this discrepancy is the choice of form factor. The moment cannot be measured directly in an antiferromagnet; one must extrapolate the measured values of $\mu f(\mathbf{Q})$ to $\mathbf{Q} = \mathbf{0}$ using a model for the form factor. A common choice in a number of early studies[19,7] was to use a smooth interpolation of the experimentally measured form factor for Cu in ferromagnetic K_2CuF_4.[37] As pointed out by Kaplan, Mahanti, and Chang,[38] this was a particularly unfortunate choice. Because of the ferromagnetism, the spin density on the

fluorine ligands contributes to the form factor at small Q; whereas, in an antiferromagnet, the spin density on a ligand positioned symmetrically between a pair of magnetic ions must be zero. Thus, the experimental form factor for K_2CuF_4 is significantly depressed (by 10% compared to both Cu $3d_{x^2-y^2}$ and spherical Cu) at the Q values where the first magnetic reflections occur in the cuprates, and hence one tends to substantially overestimate the magnetic moment.

The ordered magnetic moment μ is equal to $g\langle S\rangle$, where g is the Landé g factor. In a 2D spin-$\frac{1}{2}$ Heisenberg antiferromagnet, spin-wave theory[39,40] predicts that the average spin should be reduced by a factor of 0.606 due to zero-point spin fluctuations. (Actually, $YBa_2Cu_3O_{6+x}$ is a highly anisotropic 3D system, and the zero-point reduction should not be quite as great as this.) Taking a typical g value of 2.2, one would expect an ordered moment of roughly $0.67\mu_B$ for the case of moments completely localized on Cu. The observed reduction from this value is due to covalency. Kaplan, Mahanti, and Chang[38] have emphasized the importance of covalency effects, and suggest that a larger reduction should be expected. To properly model the effects of covalency, one must go beyond estimates of the moment, and do a proper job of calculating the form factor. Our value for the moment may be too large if the form factor flattens out substantially at small Q. A more detailed study of the Cu form factor in $Sr_2CuO_2Cl_2$ is in progress.[41]

Recognition of the anisotropy in the form factor is of significance for proper interpretation of inelastic scattering measurements. Rossat-Mignod *et al.*[17] have observed anisotropy in measurements of spin fluctuations in superconducting crystals with $x = 0.53$ and 0.92. They explained it in terms of a difference in the cross sections for fluctuations parallel and perpendicular to the CuO_2 planes. It now appears that the effect can be accounted for entirely by the **Q** dependence of the form factor.

IV. MAGNETIC DYNAMICS

In a previous paper[11] we described a spin Hamiltonian appropriate for antiferromagnetic $YBa_2Cu_3O_{6+x}$, and analyzed the spin-wave modes. We begin here with a brief summary of that model. The dominant interaction is the superexchange $J_{\|}$ between nearest-neighbor Cu sites within the CuO_2 layers. It is responsible for the very strong dispersion of spin waves propagating parallel to the layers. Spin-orbit coupling[42] results in a weak anisotropy of the superexchange, which is xy-like and of relative magnitude α_{xy}. This anisotropy leads to an energy gap for modes in which the displacements of the spins are perpendicular to the planes. The coupling $J_{\perp 1}$ between copper spins in nearest-neighbor layers (intrabilayer coupling) causes a splitting of the modes into acoustic and optical branches. The bilayer structure factor given in Eq. (4) also applies to the cross section for acoustic-mode spin waves; for the optical modes, the sine function is replaced by cosine. Finally, the weak coupling $J_{\perp 2}$ between bilayers results in a small dispersion in the Q_z direction. Below, we will first discuss measurements of the acoustic modes, and then describe the search for the optical modes. In all cases, exchange parameters were extracted by fitting inelastic scattering measurements with the spin-wave cross section, described in Ref. 11, convolved with the spectrometer resolution function.

The steep dispersion of the in-plane spin waves makes it difficult to resolve them. To do so we must make use of our knowledge of the resolution function. Although it is not possible to get a perfect alignment of the resolution function with the dispersion surface, it is nevertheless possible to optimize the orientation of the resolution function within the scattering plane.[16] This focusing effect is illustrated in Fig. 6, which shows a scan along $\mathbf{Q} = (\frac{1}{2}, \frac{1}{2}, l)$ (expressed in reciprocal lattice units) at an excitation energy of 14 meV. Besides the sinusoidal modulation due to the acoustic-mode bilayer structure factor, one can see a strong enhancement of the cross section at $l = -1.8$ relative to $l = +1.8$. The enhancement correlates with a minimum resolution width in the direction perpendicular to the $(\frac{1}{2}, \frac{1}{2}, l)$ rod. The intensity modulation is well reproduced by the calculated curve, at least in the range $-5 \lesssim l \lesssim 5$. Beyond that range deviations occur due to scattering by nonmagnetic processes, such as phonons and accidental Bragg scattering.

To measure the in-plane dispersion, we held the energy-transfer fixed (constant-E scan) and scanned **Q** across the magnetic rod in the direction (h, h, l_0). The value of l_0 was optimized at each energy transfer, using calculations of the resolution function. Figure 7 shows scans at $\hbar\omega = 14$ and 42 meV measured at a temperature of 30 K. At the higher energy, the two spin-wave branches are nearly resolved. Least-squares fits to the data, indicated by the solid curves, yield $J_{\|} = 120 \pm 20$ meV. It is important to note that this value is calculated using a cross section for classical spins. For a 2D spin-$\frac{1}{2}$ Heisenberg system, the spin-wave energies are renormalized relative to the classical results by a constant value of 1.18.[43,44] Thus, to the extent that such a description applies, the value of $J_{\|}$ should be reduced by the corresponding ratio, giving an energy of 100 ± 20 meV. As

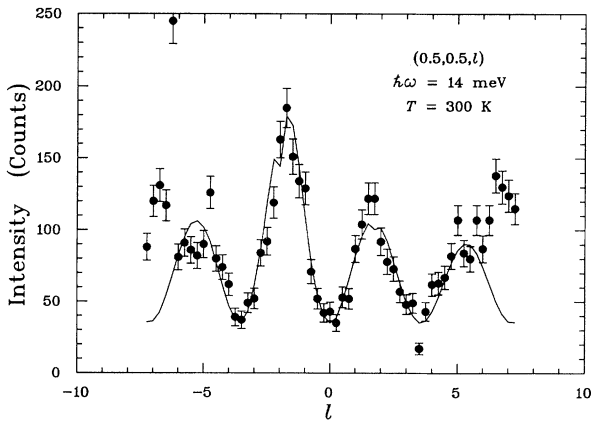

FIG. 6. Constant-E scan along the 2D magnetic rod $(\frac{1}{2}, \frac{1}{2}, l)$ at an energy transfer of 14 meV and a temperature of 300 K. The solid line is a calculation taking into account the resolution function.

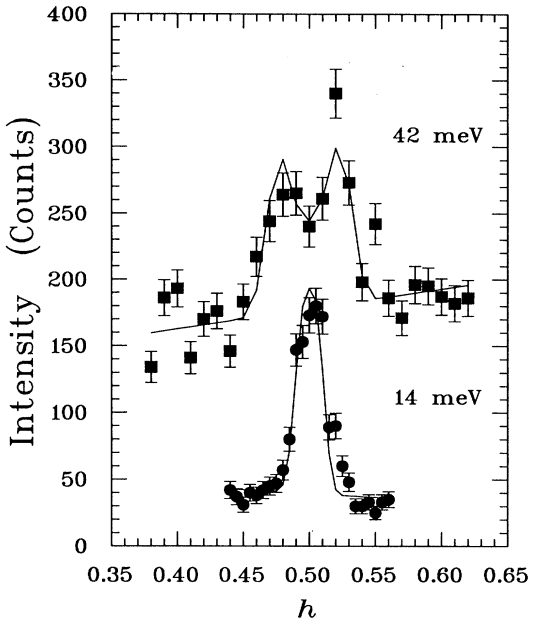

FIG. 7. Constant-E scans across the 2D magnetic rod along (h, h, l_0) at excitation energies of 14 and 42 meV, measured at 30 K with a fixed final energy of 14.7 meV. The values of l_0 are -2 and -4.9, respectively. The solid lines represent calculated intensities. The counting time was 52 min/point at 42 meV and 10.5 min/point at 14 meV.

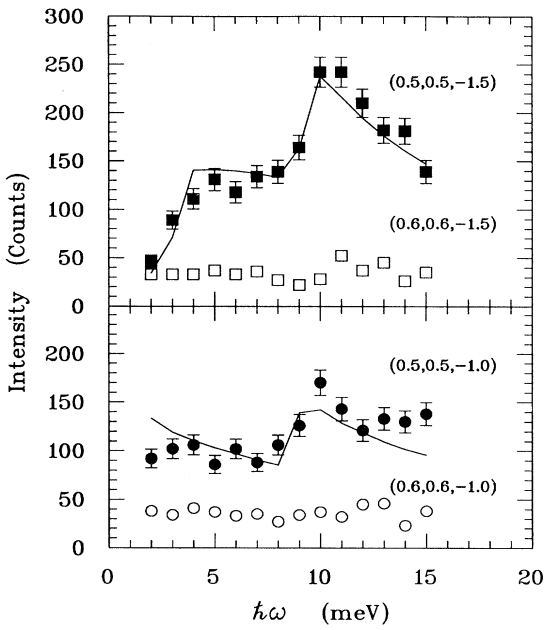

FIG. 8. Constant-Q scans at the magnetic zone center (bottom) and zone boundary along Q_z (top) measured at 30 K. The solid lines are calculated intensities; open symbols represent background.

noted earlier, the ordered state is really an anisotropic 3D system and not purely two dimensional; as a result, the renormalization effect should be somewhat reduced. The proper renormalization constant could be estimated using spin-wave theory, but we have not done so.

Our value for $J_{\|}$ in $YBa_2Cu_3O_{6.15}$ is significantly smaller than the quantum-corrected value of ~ 135 meV determined for La_2CuO_4 by neutron scattering[45–47] and two-magnon Raman scattering.[43] That it is smaller is consistent with Raman measurements on antiferromagnetic $YBa_2Cu_3O_{6+x}$.[48–50] The ratio of the two-magnon peak energies in the two materials yields a ratio of superexchange energies equal to 2700 cm^{-1}/3200 cm^{-1} = 0.84. The reduction of $J_{\|}$ in 1:2:3 is also consistent with the increase in the Cu-O bond length, which reduces the hybridization[51] (although the change in the difference in Madelung site potentials[52] partially offsets this effect). On the other hand, Rossat-Mignod and co-workers[12,13] have reported a much larger value of ~ 170 meV (without quantum correction). This value is based on measurements at $\hbar\omega$ up to 35 meV on a crystal with $x = 0.15$ in which the spin waves are not resolved. Although we do not have sufficient information to evaluate the resolution function appropriate to those measurements, we note that we can simulate spectra consistent with the reported data using our much lower value of $J_{\|}$. Thus, in the absence of a detailed justification for the much higher result, we consider it likely that the value of 170 meV is a significant overestimate for $J_{\|}$.

To determine the parameters α_{xy} and $J_{\perp 2}$ for the present crystal, constant-$\mathbf{Q}$ scans were performed at the zone-center position $(\frac{1}{2}, \frac{1}{2}, -1)$ and the zone boundary along the Q_z direction $(\frac{1}{2}, \frac{1}{2}, -1.5)$. The data collected at 30 K are shown in Fig. 8. The large anisotropy gap of ~ 9 meV and Q_z dispersion of ~ 3.5 meV are significantly larger than those observed by Rossat-Mignod and co-workers[12,13] for a similar crystal at 200 K. Part of the difference may be due to temperature dependence, as we observed a decrease of the anisotropy gap by several meV at 300 K. The anisotropy gap energy at zone center is equal to $2J_{\|}\sqrt{2\alpha_{xy}}$, while the effective gap due to Q_z dispersion is given by $\sqrt{2J_{\|}J_{\perp 2}}$. From the fits shown in the figure, we find $\alpha_{xy} = (7 \pm 1) \times 10^{-4}$ and $J_{\perp 2} = 0.04 \pm 0.01$ meV.

To search for the optical modes, we performed cross-rod constant-E scans at the position $l_0 = -7.1$, where the structure factors should be maximum for the optical and minimum for the acoustic modes. These were compared with acoustic-mode scans at $l_0 = -5.0$. At $\hbar\omega = 56$ meV we could still see a clear acoustic peak, but optical-mode measurements at 60 meV indicated no discernible signal above the background, consistent with other reports.[12,13] At 66 meV no positive signal could be identified in either channel. (At frequencies small compared to $2J_{\|}$, the spin-wave cross section falls off as $\omega_{\mathbf{q}}^{-1}$, and so magnetic scattering becomes increasingly difficult to detect as the excitation energy increases.) The minimum optical-mode energy should be equal to $2\sqrt{J_{\|}J_{\perp 1}}$. Taking 60 meV as a lower limit for this quantity, we obtain a lower limit for $J_{\perp 1}$ of 8 meV.

V. INTEGRATED INTENSITIES

When holes are doped into the antiferromagnetic CuO_2 layers, the magnetic scattering is significantly modified.

It is not easy to put the resulting diffuse inelastic scattering cross section on an absolute scale; however, we can do so indirectly by making a comparison with the scattering strength in the antiferromagnetic phase, where spin-wave theory appears to work quite well. In this section we will first discuss a form of integrated intensity for antiferromagnetic $YBa_2Cu_3O_{6.15}$, and then compare with results obtained previously for a crystal with $x = 0.6$ and $T_c = 53$ K.[16]

Neutron scattering measures a scattering function $S(\mathbf{Q},\omega)$, which is related to the imaginary part of the dynamical susceptibility by the dissipation-fluctuation theorem:

$$S(\mathbf{Q},\omega) = \frac{1}{1-e^{-\hbar\omega/kT}}\,\chi''(\mathbf{Q},\omega). \tag{7}$$

For a 2D square-lattice spin-$\frac{1}{2}$ Heisenberg antiferromagnet with only nearest-neighbor exchange J, χ'' (per Cu atom) is given by

$$\chi''(\mathbf{Q},\omega) = \frac{1}{2}\frac{1+\gamma_{\mathbf{q}}}{\sqrt{1-\gamma_{\mathbf{q}}^2}}\,\delta(\hbar\omega-\hbar\omega_{\mathbf{q}}), \tag{8}$$

where

$$\omega_{\mathbf{q}} = 2J\sqrt{1-\gamma_{\mathbf{q}}^2}, \tag{9}$$

$$\gamma_{\mathbf{q}} = \frac{1}{2}(\cos q_x a + \cos q_y a), \tag{10}$$

and

$$\mathbf{q} = \mathbf{Q} - \mathbf{G}_{\mathrm{AF}}, \tag{11}$$

with $\mathbf{G}_{\mathrm{AF}}$ being a reciprocal lattice vector of the antiferromagnetic lattice and a the nearest-neighbor spacing. When the quantity qa is small, one obtains the approximate formula

$$\chi''(\mathbf{Q},\omega) \approx \frac{1}{\sqrt{2}qa}\,\delta(\hbar\omega-\hbar cq), \tag{12}$$

where the spin-wave velocity c times $\hbar$ is equal to $\sqrt{2}Ja$. It has been pointed out[53] that the 2D $\mathbf{q}$ integral of the right-hand side of Eq. (12) [which we will label $\tilde{\chi}''(\omega)$] is a constant; specifically, it is equal to π/Ja^2. Now at $T = 0$ the temperature factor in Eq. (7) is equal to 1, and the integral of $S(\mathbf{Q},\omega)$, which we will label $\tilde{S}(\omega)$, will also be independent of frequency. At finite temperatures, the frequency dependence is determined by the temperature factor.

Although the exchange in $YBa_2Cu_3O_{6.15}$ is not perfectly isotropic and a weak interbilayer coupling exists, one would still expect the frequency independence of $\tilde{S}(\omega)$ to be observed for the acoustic modes at low temperatures and at energies greater than the anisotropy gap. To test this we measured cross-rod scans for $9 \le \hbar\omega \le 26$ meV at $(\frac{1}{2},\frac{1}{2},-2)$ and for $26 \le \hbar \le 56$ meV at $(\frac{1}{2},\frac{1}{2},-5)$, using a fixed final neutron energy of 30.5 meV. One of the 2D $\mathbf{q}$ components is normal to the horizontal scattering plane, and because of the relaxed collimation in that direction, the resolution function essentially integrates over that component. Hence, to complete the 2D integral, we only have to do a one-dimensional integral of the measured intensity along the direction of the scan. The measurements at different l positions were normalized by correcting for the bilayer structure factor and the calculated magnetic form factor. The results obtained at 9 K and 300 K are shown in Fig. 9. As expected, $\tilde{S}(\omega)$ at 9 K is a constant (indicated by the solid line), and at 300 K $\tilde{S}(\omega)$ is equal to that same constant times the temperature factor (indicated by the long-dashed line).

To compare measurements on the $x = 0.6$ crystal, it is necessary to correct for differences in crystal volume. This normalization was done using the integrated intensities for longitudinal acoustic phonons measured near (006). The ratio of volumes for $x = 0.6$ relative to 0.15 was found to be 1.35 ± 0.3. The normalized $x = 0.6$ data obtained at 10 K are included in Fig. 9. (The normalization uncertainty is not included in the error bars.) One can see that while $\tilde{S}(\omega)$ for the superconducting sample is suppressed at low energies, it rises to roughly 3 times the spin-wave value at its peak near 30 meV.

Our reason for comparing $\tilde{S}(\omega)$ rather than $\tilde{\chi}''(\omega)$ is that a useful sum rule exists for S:

$$\int d\mathbf{Q}d\omega\, S(\mathbf{Q},\omega) = s(s+1), \tag{13}$$

where $s = \frac{1}{2}$ is the spin. Note that the integral over frequency includes the magnetic Bragg peak component at $\omega = 0$ as well as the inelastic spin-wave scattering. The weight in the Bragg peak is $\langle s_z\rangle^2$, and with $\langle s_z\rangle \approx 0.3$ at $T = 0$, the Bragg peak accounts for only about 10% of the total sum. The rest of the spectral weight is spread over an energy range extending up to $2J$ (≈ 240 meV). With increasing temperature, Bragg intensity is trans-

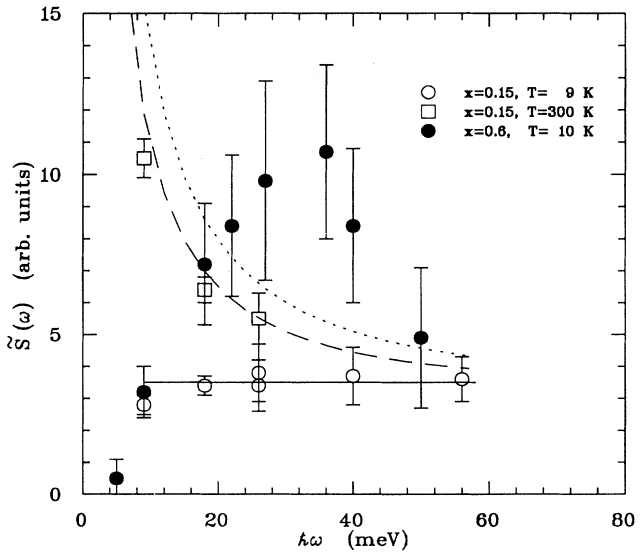

FIG. 9. Variation of $\tilde{S}$ with $\hbar\omega$. The open symbols correspond to measurements on $YBa_2Cu_3O_{6.15}$ at 9 K (circles) and 300 K (squares). The solid circles represent previous measurements (Ref. 16) on $YBa_2Cu_3O_{6.6}$ at 10 K. The uncertainty due to the phonon normalization is not included in the error bars. The lines are discussed in the text.

ferred to the low-energy range with a distribution determined by the temperature factor. The short-dashed line in Fig. 9 indicates an extrapolation of the spin-wave measurements to 400 K, where essentially all of the spectral weight should be inelastic. In the metallic sample there is no elastic component, and so it is probably most meaningful to compare with the high-temperature extrapolation for the antiferromagnet.

Without knowledge of the spectral weight for the metallic sample at higher energies, it is not possible to make direct use of the sum rule. Nevertheless, one can see that the spectral weight for $\hbar\omega < 50$ meV is quite comparable in the antiferromagnet and the superconductor. The dominant change caused by doping appears to be a shift in weight from $\hbar\omega \sim 0$ out to ~ 30 meV.

The normalization to the spin-wave results makes possible a comparison of χ'' in the metallic sample with results obtained from nuclear magnetic resonance studies. Mehring[54] has defined a quantity

$$I_{\mathbf{G}_{\mathrm{AF}}} \equiv \sum_{\mathbf{q}} \frac{\chi''(\mathbf{q},\omega_0)}{\hbar\omega_0}, \tag{14}$$

where ω_0 is the nuclear Larmor frequency and the sum is over the antiferromagnetic Brillouin zone centered on the magnetic reciprocal lattice vector $\mathbf{G}_{\mathrm{AF}}$. For $YBa_2Cu_3O_{6.6}$ with $T_c = 60$ K, he extracts a value for $I_{\mathbf{G}_{\mathrm{AF}}}$ of 33.2 eV^{-2} at a temperature of 200 K. If $\chi''(\mathbf{q},\omega)$ is linear in frequency over some range, then $I_{\mathbf{G}_{\mathrm{AF}}}$ will be independent of the choice of ω_0, and we can evaluate this quantity using neutron data. For our $T_c = 53$ K crystal,[16] the only temperature at which χ'' appears linear in ω and at which we have sufficient data for comparison is 100 K. At that temperature χ'' appears to be approximately linear for $\hbar\omega \lesssim 10$ meV. At $\hbar\omega = 9$ meV, the 2D $\mathbf{q}$-integrated susceptibility $\tilde{\chi}''$ is equal to roughly 60% of the 10 K value, and the latter value is approximately equal to the spin-wave result, as shown in Fig. 9. To put $\tilde{\chi}''$ on an absolute scale, we take the value $\pi/J_{\|}a^2$ for a single-layer Heisenberg system and divide by 2, because in 1:2:3 only half of the spin-wave modes contribute at low energy. (This corresponds to averaging the bilayer structure factor over Q_z.) For $I_{\mathbf{G}_{\mathrm{AF}}}$, we then have

$$I_{\mathbf{G}_{\mathrm{AF}}} = 0.6 \times \frac{1}{2} \times \left(\frac{\pi}{J_{\|}a^2}\right) \times \left(\frac{a}{2\pi}\right)^2 \div (9\ \mathrm{meV}), \tag{15}$$

where the division by $(2\pi/a)^2$, the area of a Brillouin zone, is needed to convert $\tilde{\chi}''$ to an average over $\mathbf{q}$. Plugging in $J_{\|} = 120$ meV gives $I_{\mathbf{Q}_{\mathrm{AF}}} = 22\ \mathrm{eV}^{-2}$, which is quite consistent with Mehring's value, considering the differences in samples and temperatures, and the large uncertainty in our result.

The finding that the average of χ'' near $\mathbf{G}_{\mathrm{AF}}$ measured by neutrons and NMR is comparable is an important one. It indicates that both techniques are probing the same antiferromagnetic fluctuations, and that some sort of interpolation between the very low frequency NMR regime and the moderate frequency neutron range should be possible. We hope to extend the normalization procedure to other superconducting samples in future work.

ACKNOWLEDGMENTS

One of the authors (S.S.) gratefully acknowledges the kind hospitality of the members of the neutron-scattering group at Brookhaven during his stay. This study was supported by the U.S.–Japan collaborative Program on Neutron Scattering, and by a Grant-in-Aid for Scientific Research from the Ministry of Education, Science and Culture. Work at Brookhaven was carried out under Contract No. DE-AC02-76CH00016, Division of Materials Sciences, U.S. Department of Energy.

[1] S. Chakravarty, in *High Temperature Superconductivity*, edited by K. Bedell, D. Coffey, D. E. Meltzer, D. Pines, and J. R. Schrieffer (Addison-Wesley, Redwood City, CA, 1990), pp. 136–187.

[2] R. J. Birgeneau and G. Shirane, in *Physical Properties of High Temperature Superconductors*, edited by D. M. Ginsberg (World Scientific, Singapore, 1989), pp. 151–211.

[3] J. D. Jorgensen, B. W. Veal, A. P. Paulikas, L. J. Nowicki, G. W. Crabtree, H. Claus, and W. K. Kwok, Phys. Rev. B **41**, 1863 (1990).

[4] R. J. Cava, A. W. Hewat, E. A. Hewat, B. Batlogg, M. Marezio, K. M. Rabe, J. J. Krajewski, J. W. F. Peck, and J. L. W. Rupp, Physica C **419**, 419 (1990).

[5] J. M. Tranquada, D. E. Cox, W. Kunnmann, H. Moudden, G. Shirane, M. Suenaga, P. Zolliker, D. Vaknin, S. K. Sinha, M. S. Alvarez, A. J. Jacobson, and D. C. Johnston, Phys. Rev. Lett. **60**, 156 (1988).

[6] J. Rossat-Mignod, P. Burlet, M. J. Jurgens, C. Vettier, L. P. Regnault, J. Y. Henry, C. Ayache, L. Forro, H. Noel, M. Potel, P. Gougeon, and J. C. Levet, J. Phys. (Paris) Colloq. **49**, C8-2119 (1988).

[7] J. M. Tranquada, A. H. Moudden, A. I. Goldman, P. Zolliker, D. E. Cox, G. Shirane, S. K. Sinha, D. Vaknin, D. C. Johnston, M. S. Alvarez, A. J. Jacobson, J. T. Lewandowski, and J. M. Newsam, Phys. Rev. B **38**, 2477 (1988).

[8] M. J. Jurgens, P. Burlet, C. Vettier, L. P. Regnault, J. Y. Henry, J. Rossat-Mignod, H. Noel, P. Gougeon, and J. C. Levet, Physica B **156&157**, 846 (1989).

[9] L. Rebelsky, J. M. Tranquada, G. Shirane, Y. Nakazawa, and M. Ishikawa, Physica C **160**, 197 (1989).

[10] M. Sato, S. Shamoto, J. M. Tranquada, G. Shirane, and B. Keimer, Phys. Rev. Lett. **61**, 1317 (1988).

[11] J. M. Tranquada, G. Shirane, B. Keimer, S. Shamoto, and M. Sato, Phys. Rev. B **40**, 4503 (1989). There are some missing factors of 2 in Table I of this paper, as well as some minor errors in Eqs. (13) and (14).

[12] C. Vettier, P. Burlet, J. Y. Henry, M. J. Jurgens, G. Lapertot, L. P. Regnault, and J. Rossat-Mignod, Phys. Scr. T **29**, 110 (1989).

[13] J. Rossat-Mignod, J. X. Boucherle, P. Burlet, J. Y. Henry, J. M. Jurgens, G. Lapertot, L. P. Regnault, J. Schweizer,

F. Tasset, and C. Vettier, in *International Seminar on High Temperature Superconductivity, Dubna, USSR, 1989*, edited by V. L. Aksenov, N. M. Bogolubov, and N. M. Plakida (World Scientific, Singapore, 1990), pp. 74–85.
[14]H. Chou, J. M. Tranquada, G. Shirane, T. E. Mason, W. J. L. Buyers, S. Shamoto, and M. Sato, Phys. Rev. B **43**, 5554 (1991).
[15]J. Rossat-Mignod, L. P. Regnault, C. Vettier, P. Burlet, J. Y. Henry, and G. Lapertot, Physica B **169**, 58 (1991).
[16]J. M. Tranquada, P. M. Gehring, G. Shirane, S. Shamoto, and M. Sato, Phys. Rev. B **46**, 5561 (1992).
[17]J. Rossat-Mignod, L. P. Regnault, C. Vettier, P. Bourges, P. Burlet, J. Bossy, J. Y. Henry, and G. Lapertot, Physica B **180&181**, 383 (1992).
[18]H. A. Mook, M. Yethiraj, G. Aeppli, T. E. Mason, and T. Armstrong, Phys. Rev. Lett. **70**, 3490 (1993).
[19]T. Freltoft, G. Shirane, S. Mitsuda, J. P. Remeika, and A. S. Cooper, Phys. Rev. B **37**, 137 (1988).
[20]X. L. Wang, L. L. Miller, J. Ye, C. Stassis, B. N. Harmon, D. C. Johnston, A. J. Schultz, and C. Loong, J. Appl. Phys. **67**, 4524 (1990).
[21]H. Kadowaki, M. Nishi, Y. Yamada, H. Takeya, H. Takei, S. M. Shapiro, and G. Shirane, Phys. Rev. B **37**, 7932 (1988).
[22]J. W. Lynn, W. Li, H. A. Mook, B. C. Sales, and Z. Fisk, Phys. Rev. Lett. **60**, 2781 (1988).
[23]A. H. Moudden, G. Shirane, J. M. Tranquada, R. J. Birgeneau, Y. Endoh, K. Yamada, Y. Hidaka, and T. Murakami, Phys. Rev. B **38**, 8720 (1988).
[24]W. Li, J. W. Lynn, and Z. Fisk, Phys. Rev. B **41**, 4098 (1990).
[25]A. H. Moudden, P. Schweiss, B. Hennion, P. M. Gehring, G. Shirane, and Y. Hidaka, Physica C **185–189**, 1167 (1991).
[26]S. Shamoto and M. Sato, Physica C **185–189**, 465 (1991).
[27]K. Zhang, B. Dabrowski, C. U. Segre, D. G. Hinks, I. K. Schuller, J. D. Jorgensen, and M. Slaski, J. Phys. C **20**, L935 (1987).
[28]S. Li, E. A. Hayri, K. V. Ramanujachary, and M. Greenblatt, Phys. Rev. B **38**, 2450 (1988).
[29]T. Iwata, Y. Tajima, and M. Hikita, J. Cryst. Growth **91**, 274 (1988).
[30]H. Lütgemeier and B. Rupp, J. Phys. (Paris) Colloq. **49**, C8-2147 (1988).
[31]J. M. Tranquada, S. M. Heald, A. R. Moodenbaugh, and Y. Xu, Phys. Rev. B **38**, 8893 (1988).
[32]H. Tolentino, F. Baudelet, A. Fontaine, T. Gourieux, G. Krill, J. Y. Henry, and J. Rossat-Mignod, Physica C **192**, 115 (1992).
[33]J. M. Tranquada and G. Shirane, Physica C **162–164**, 849 (1989).
[34]A. J. Freeman, Acta Crystallogr. **12**, 261 (1959).
[35]A. J. Freeman, Phys. Rev. **113**, 169 (1959).
[36]J. W. Davenport, M. Weinert, and R. E. Watson, Phys. Rev. B **32**, 4876 (1985).
[37]J. Akimitsu and Y. Ito, J. Phys. Soc. Jpn. **40**, 1621 (1976).
[38]T. A. Kaplan, S. D. Mahanti, and H. Chang, Phys. Rev. B **45**, 2565 (1992).
[39]P. W. Anderson, Phys. Rev. **86**, 694 (1952).
[40]T. Oguchi, Phys. Rev. **117**, 117 (1960).
[41]J. M. Tranquada and M. Matsuda (unpublished).
[42]N. E. Bonesteel, Phys. Rev. B **47**, 11302 (1993).
[43]R. R. P. Singh, P. A. Fleury, K. B. Lyons, and P. E. Sulewski, Phys. Rev. Lett. **62**, 2736 (1989).
[44]C. M. Canali and S. M. Girvin, Phys. Rev. B **45**, 7127 (1992).
[45]G. Aeppli, S. M. Hayden, H. A. Mook, Z. Fisk, S. Cheong, D. Rytz, J. P. Remeika, G. P. Espinosa, and A. S. Cooper, Phys. Rev. Lett. **62**, 2052 (1989).
[46]S. M. Hayden, G. Aeppli, H. A. Mook, S. Cheong, and Z. Fisk, Phys. Rev. B **42**, 10220 (1990).
[47]S. M. Hayden, G. Aeppli, R. Osborn, A. D. Taylor, T. G. Perring, S. Cheong, and Z. Fisk, Phys. Rev. Lett. **67**, 3622 (1991).
[48]K. B. Lyons, P. A. Fleury, L. F. Schneemeyer, and J. V. Waszczak, Phys. Rev. Lett. **60**, 732 (1988).
[49]S. Sugai, in *Mechanisms of High Temperature Superconductivity*, edited by H. Kamimura and A. Oshiyama (Springer-Verlag, Berlin, 1989), p. 207.
[50]D. Reznik, M. V. Klein, W. C. Lee, D. M. Ginsberg, and S. Cheong, Phys. Rev. B **46**, 11725 (1992).
[51]Y. Tokura, S. Koshihara, T. Arima, H. Takagi, S. Ishibashi, T. Ido, and S. Uchida, Phys. Rev. B **41**, 11657 (1990).
[52]J. B. Torrance and R. M. Metzger, Phys. Rev. Lett. **63**, 155 (1989).
[53]S. M. Hayden, G. Aeppli, H. Mook, D. Rytz, M. F. Hundley, and Z. Fisk, Phys. Rev. Lett. **66**, 821 (1991).
[54]M. Mehring, Appl. Magn. Res. **3**, 383 (1992).